Evaluation of superabrasive grinding points for the machining of hardened steel

Hood, Richard; Medina Aguirre, Fernanda; Soriano Gonzalez, Luis; Novovic, Donka; Soo, Sein Leung

DOI:
10.1016/j.cirp.2019.04.090

Contents lists available at SciVerse ScienceDirect

CIRP Annals Manufacturing Technology

Journal homepage: www.elsevier.com/locate/cirp

Evaluation of superabrasive grinding points for the machining of hardened steel

Richard Hood [a], Fernanda Medina Aguirre [a], Luis Soriano Gonzalez [a], Donka Novovic [b], Sein Leung Soo (1)[a,*]

[a] *Machining Research Group, Department of Mechanical Engineering, School of Engineering, University of Birmingham, Edgbaston, Birmingham, B15 2TT, UK*
[b] *Manufacturing Technology, Global Manufacturing Centre, Rolls-Royce plc, Derby, DE24 8ER, UK*

Small diameter grinding points offer greater flexibility for machining free-form contours compared to traditional grinding wheels, despite fewer effective cutting edges. The paper evaluates the influence of grit size (B32, B46, B76), feed rate (125, 250 mm/min) and depth of cut (20, 40 μm) when machining D2 tool steel using electroplated CBN grinding points. Highest G-ratios (~2441) were obtained using B32 tools with corresponding workpiece surface roughness (Ra) of ~0.8 μm after ~6000 mm^3 material removed, due to the greater number of effective cutting edges. Attritious wear was the primary wear mechanism although material loading was observed with B76 tools.

Grinding; Cubic boron nitride (CBN); Wear

1. Introduction

In production of critical steel components, hard finish machining is a necessary step not only to reduce form and surface defects that arise due to heat treatment, but also to ensure that dimensional accuracy as well as surface quality requirements are met. Grinding is the most commonly utilised process for finishing of hard materials due to its ability for achieving geometrical tolerances down to <10 μm, and generating a surface finish of <Ra 0.5 μm [1]. However, increasing demands in the aerospace industry continue to test the limits of current grinding technology, particularly for finishing free-form surfaces. Hence, development of flexible/cost-effective solutions to address such challenges are necessary. Abrasive machining using small diameter wheels/grinding points (< 25 mm) is a potential option for generating and finishing complex contours/features in parts where high surface quality is a critical requirement. Nevertheless, the reduction in tool size poses a number of process drawbacks, not least limiting the maximum achievable cutting speed as well as the number of effective cutting edges interacting with the ground surface, which can lead to detrimental effects such as increased vibration, excessive wheel wear, low accuracy and deterioration of workpiece surface quality.

Publications concerning machining using grinding points (also commonly known as point grinding) is relatively limited, with the majority focusing on nickel and titanium aerospace alloys as well as some ferrous materials, although none have featured steels in the hardened state. Early work to evaluate the feasibility of utilising plain electroplated grinding points (~15 mm diameter) mounted on a high-speed machining centre (60,000 rpm) to machine Udimet 720 and Inconel 718 was reported by Aspinwall et al. [2]. The effect of grit size, grit material, grit toughness, wheel speed, depth of cut, feed rate and fluid pressure on workpiece surface roughness and tool wear was investigated. Grit size had the greatest influence on surface roughness followed by depth of cut, feed rate, and wheel speed while the remaining factors showed no significant/negligible effect. Further development employing fir tree-profiled grinding points operating at 60,000 and 90,000 rpm on Udimet 720 workpieces was carried out to assess the influence of different grit size and type on surface roughness and wheel wear [3]. Results showed that increasing cutting speed led to reduced tool wear rates while cubic boron nitride (CBN) grits produced lower absolute wear levels compared to diamond, albeit at the expense of higher workpiece surface roughness. More recently, work carried out by Curtis et al. [4] similarly assessed the performance of electroplated CBN and diamond grinding points when machining Udimet 720 in terms of G-ratio and the subsequent influence on workpiece surface roughness/integrity. Research on point grinding of titanium alloys have included the use of electroplated [4] or vitrified bonded [5, 6] superabrasives (CBN and diamond); and vitrified corundum Al_2O_3 points [7]. Depending on the wheel characteristics and process parameters employed, ground workpiece surface roughness values varied between Ra 0.25 to 2.8 μm. Experimental work relating to grinding of ferrous materials using CBN mounted points have involved evaluating the influence of bond type [8] as well as process strategy [9] on workpiece surface roughness. When point grinding cast iron, Yan and Zhang [8] highlighted that bond material had a considerable effect on resulting surface roughness with Rz values of ~3 μm, ~9 μm and ~10 μm recorded when using vitrified, metal and resin bonded tools respectively. Uhlmann et al. [9] achieved a 50% reduction in surface roughness (Ra ~1.8 to ~0.9 μm) when grinding a tool steel (37±2 HRC) by increasing the angle formed between the feed rate and cutting speed directions from 0° to 30°.

In the current work, the performance of electroplated CBN grinding points with different grit sizes was investigated when machining hardened steel. A bespoke technique to characterise the topography of the grinding points and determine distribution, size and number of effective cutting grits was also developed to support analysis of resultant workpiece surface quality.

2. Experimental procedure

Grinding tests were conducted on a high-speed vertical machining centre (Matsuura LX1) with a maximum spindle power of 4.5 kW and speed range of 200 – 60,000 rpm. Hardened D2 tool steel (62 HRC) was used as the workpiece material. Rectangular block samples measuring 8 mm thick and 73.5 mm long were held in position using a bespoke fixture, which was clamped onto a piezoelectric three-component Kistler force dynamometer, see experimental setup in Fig. 1a. Tapered electroplated CBN grinding points at three different grit sizes (B76, B46, and B32) were

evaluated. Plunge grinding trials in a down grinding mode were performed at a fixed rotational speed of 40,000 rpm (maximum peripheral cutting speed ~11 m/s). A schematic of the grinding point detailing the dimensions and grinding region is shown in Fig. 1b. Two different combinations of radial depth of cut (a_e) and feed rate (v_f) were set: (i) a_e = 20 µm and v_f = 250 mm/min, (ii) a_e = 40 µm and v_f = 125 mm/min; in order to provide different undeformed chip thicknesses while keeping a constant material removal rate of 40 mm³/s. The end of test criterion was 6000 mm³ of workpiece material ground. All tests were undertaken wet using Hocut 3380 water-based emulsion (~7% oil concentration), which was supplied via two external nozzles (outlet diameter of 4 mm) at a flow rate of ~21 l/min.

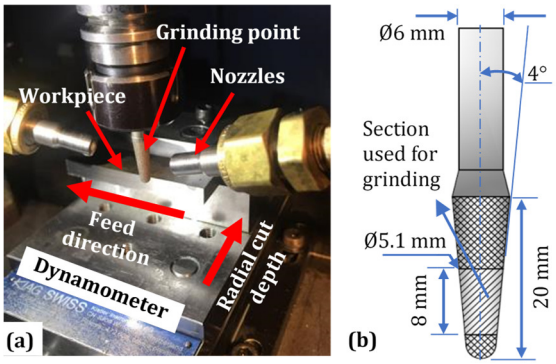

Fig. 1. (a) Experimental setup; (b) Schematic of grinding point.

Diametric tool wear was determined by measuring profiles cut in graphite replicas (3 mm thick) at predefined intervals during each test, using an Alicona InfiniteFocus microscope installed with image post-processing software. In-situ assessment of workpiece surface roughness (Ra) measured perpendicular to feed direction were carried out at regular intervals by taking the average of 9 readings at different locations along the ground surface using a Mitutoyo profilometer. Five sampling lengths each at a cut-off distance of 0.8 mm was used. Force signals from the dynamometer were processed using Dynoware software.

3. Tool surface topography characterisation

Prior to test commencement, the topography of the grinding points were characterised by scanning 8 regions (each over an area of 7.6 x 0.814 mm) around the tool circumference using the Alicona InfiniteFocus microscope. Average data from the scans were used to generate bearing ratio/Abbott-Firestone curves for the 3 different grit sizes together with associated surface texture parameters including surface roughness (Sa) and mean height of peaks (Spk). Additionally, AutoCAD® software was employed to produce contours of grits from the scanned images, with average projected grit areas (A_p) calculated based on 200 grits from each tool. The equivalent grit diameter (d_e) was then estimated by approximating to a circular shape with the same area.

Abbott-Firestone curves describe the topography of the grinding tools by showing the percentage of grit material above a specified height. The slope of the curves provide an indication of the grinding point structure/grit density, where steeper gradients correspond to a more open wheel structure and vice versa. Fig. 2 shows that the B76 tools had the lowest grit density but the highest peaks (up to ~63 µm) followed the B46 points with peak heights of up to ~51 µm, whereas the B32 tools exhibited a more closed/dense structure with maximum peaks up to ~37 µm.

Micrographs together with the measured Sa, d_e and A_p values for the different grinding points are displayed in Fig. 3. The d_e of the B32 points were 38% and 31% smaller than the B76 and B46 tools respectively. Likewise, the Sa (~4.6 µm) was found to be 52% and 39% lower than the B76 and B46 tools respectively.

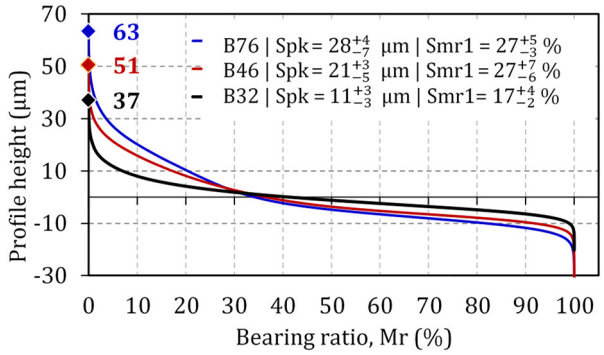

Fig. 2. Abbott-Firestone curves | **Spk:** mean height of the peaks; **Smr1:** fraction of the surface which consists of peaks above the core material.

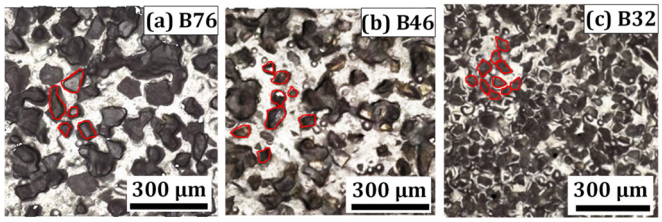

$S_a = 9.5^{+1.4}_{-1.3}$ µm, $d_e = 73^{+37}_{-22}$ µm, $A_p = 4165$ µm²

$S_a = 7.5^{+1.2}_{-1.3}$ µm, $d_e = 65^{+20}_{-29}$ µm, $A_p = 3313$ µm²

$S_a = 4.6^{+0.5}_{-0.4}$ µm, $d_e = 45^{+20}_{-29}$ µm, $A_p = 1557$ µm²

Fig. 3. Surface topography parameters for new (a) B76; (b) B46; (c) B32 grinding points. Instrument: Alicona InfiniteFocus |Magnification: 20X |Vertical resolution: 0.581 µm | Lateral resolution: 7.57µm.

4. Results and discussion

4.1. Tool wear

The evolution of tool diametric wear with respect to volume of material removed is shown in Fig. 4. In general, variation in cutting conditions did not appear to cause a significant difference in terms of wear progression for each of the grit sizes. The coarser grit tools (B76) exhibited the highest initial diametric wear of up to ~50 µm, followed by a gradual wear rate until failure after ~4700 mm³ of material removed due to wheel loading and excessive diametric wear of up to ~78 µm. In contrast, the B46 and B32 tools displayed lower initial wear of up to ~40 µm and ~25 µm respectively.

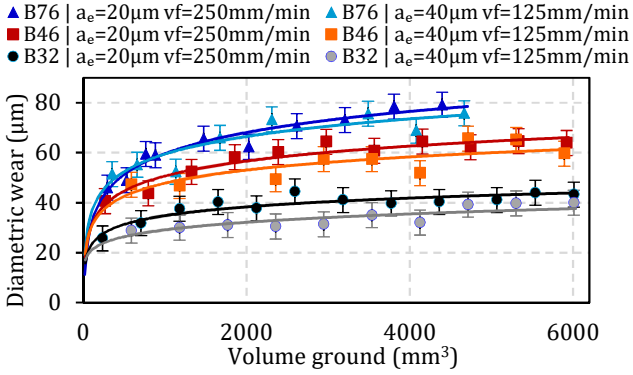

Fig. 4. Grinding point wear progression.

All tests involving B46 and B32 tools successfully ground ~6000 mm³ of material, with corresponding tool wear levels of ~62

µm and ~42 µm respectively. In terms of G-ratios, the B32 wheels outperformed the B76 tools by ~132% (~2441 vs. ~1051).

Fig. 5. details comparative 3D surface topography maps of new and worn grinding points used in trials at low feed rate/high depth of cut (125 mm/min and 40 µm). The worn tool surfaces typically showed a decrease in mean peak height (Spk) of between 71% and 82% when compared to those in the new condition. The average grain height of the worn tools (based on measurement scans at 8 different locations around the periphery) at the end of each test is detailed in Fig. 6. Despite similar diametric wear levels recorded for the B76 tools (see Fig. 4), the average Spk of the tool surface following the test at a_e = 40 µm and v_f = 125 mm/min (smaller undeformed chip thickness) was approximately twice the value obtained in the corresponding trial (20 µm and 250 mm/min). This was due to the wider range of mean peak height values (between ~8 and ~18 µm) obtained in the former, indicating highly uneven distribution of grit wear around the tool circumference. Similarly, the Spk measurements varied between ~5 and 10 µm in the B46 tools, which was most likely due to tool runout.

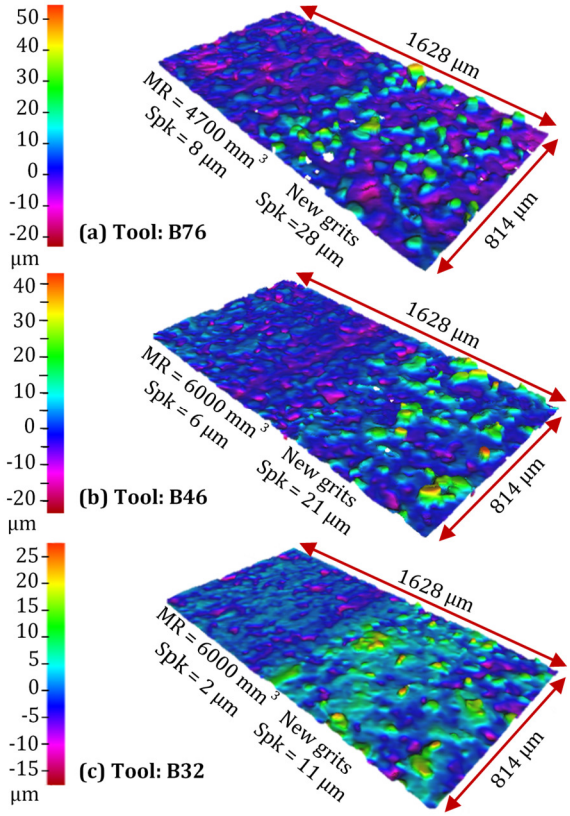

Fig. 5. Sample 3D surface topography maps of new and worn tools| a_e = 40 µm, v_f =125 mm/min: (a) B76; (b) B46; (c) B32.

Grain pull-out and attritious wear were the principal wear mechanisms observed on all of the tool surfaces, regardless of grain size as evidenced by the contour plots in Fig. 7. Heavy wheel loading was also seen on the B76 tool used in the trial involving high feed rate/low depth of cut combination, see Fig. 7a. This was attributed to the rapid build-up/adhesion of workpiece chips over the larger wear flat areas on B76 grits, which formed as a consequence of increased frictional forces due to the greater chip thickness resulting from the higher feed rate (250 mm/min) employed. Furthermore, the considerable grain loss and attritious wear also led to rubbing between the bond and workpiece on the worn B46 and B32 tool surfaces, which are apparent in Figs. 7b and 7c.

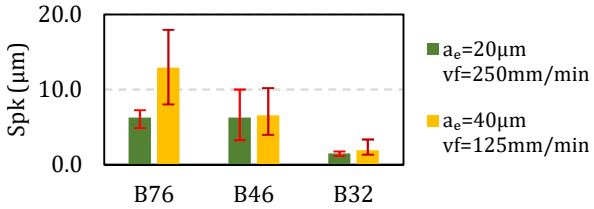

Fig. 6. Average grain height of the grinding points at test cessation.

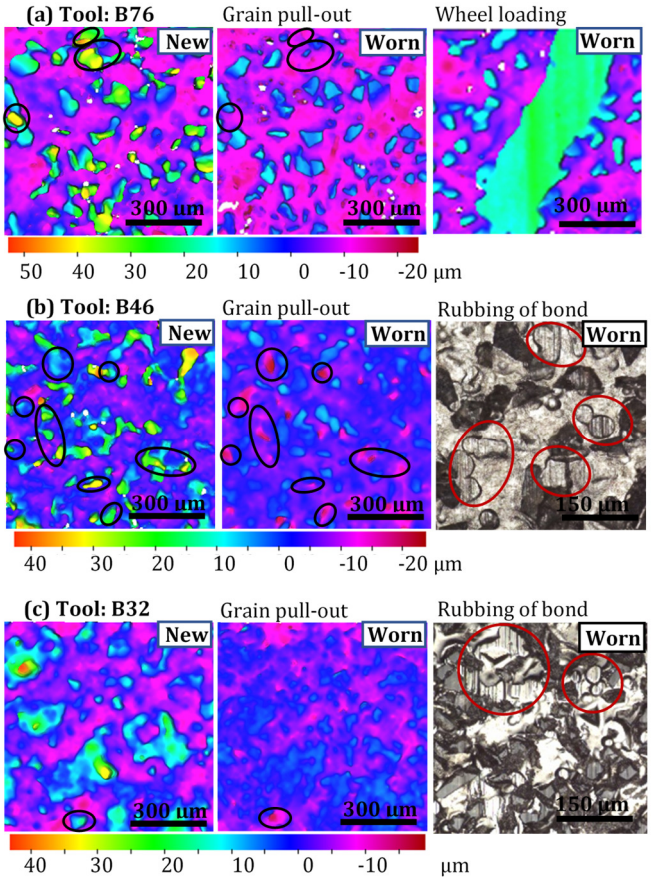

Fig. 7. Contour plots and micrographs of grinding points in new and worn condition| a_e = 20 µm, v_f =250 mm/min: (a) B76; (b) B46; (c) B32.

4.2. Workpiece surface roughness

Workpiece surface roughness (Ra) measured over the experimental duration are presented in Fig. 8, which show the typical trend of high initial values followed by a gradual decrease with increasing material removed until a steady state/plateau due to conditioning/dulling of the grits. Unlike B46 and B32 tools, a considerable difference in workpiece roughness was observed between the two tests involving B76 grinding points. Despite a smaller undeformed chip thickness and extended contact length, the low feed rate/high depth of cut parameter combination (125 mm/min and 40 µm) unexpectedly generated ~45% higher surface roughness (~1.4 vs. 0.9 µm Ra). This was likely the consequence of the uneven wear distribution resulting from the greater tool run-out highlighted previously in Section 4.1.

It was observed that a larger spread of tool Spk values (uneven wear distribution) generally correlated with higher workpiece Ra, as in the case of both B46 tools and B76 operating at a_e = 40 µm and v_f = 125 mm/min, see Figs. 6 and 8. While the B32 tools generated the best workpiece roughness as anticipated (Ra ~0.8 µm), the B76 tool grinding at a_e = 40 µm and v_f = 250 mm/min also

produced comparable workpiece Ra ~0.9 µm. All 3 grinding points had uniform wear with maximum Spk variation of ~2 µm.

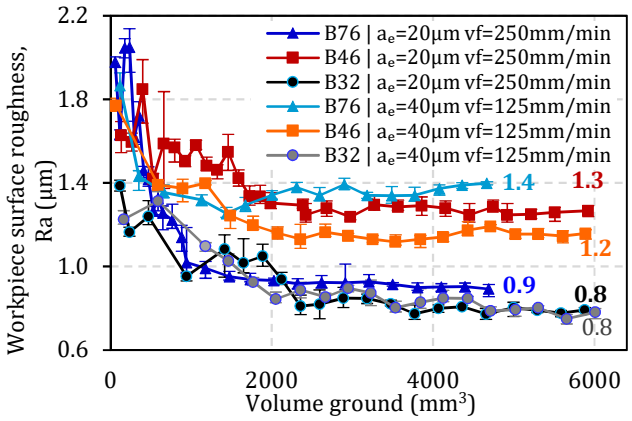

Fig. 8. Workpiece surface roughness progression.

4.3. Cutting forces

Root mean square (RMS) amplitudes of resultant cutting forces with associated maximum and minimum values over the volume ground are detailed in Fig. 9. In general, initial grinding forces were relatively low (<4 N/mm) but increased with tool wear. Leaving aside the B76 tests, forces at test cessation were 30% lower for trials at a_e = 40 µm and v_f = 125 mm/min (~7 vs. ~10 N/mm). In contrast, forces of up to ~13 N/mm were observed for the loaded B76 tool operating at a_e = 20 µm and v_f = 250 mm/min.

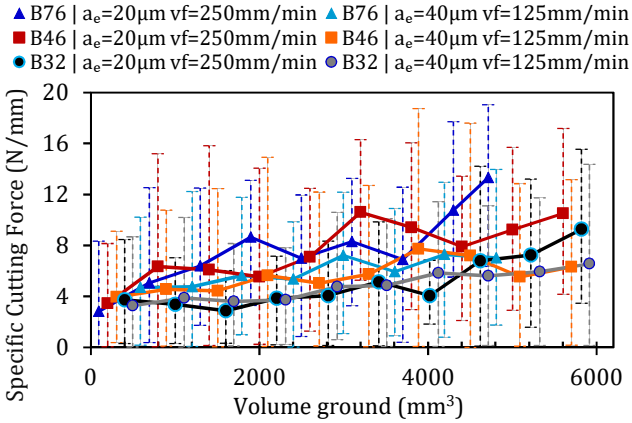

Fig. 9. Resultant cutting forces (RMS).

4.4. Effective cutting grains

Ground surface quality depends primarily on the workpiece-grinding wheel interaction. The effective cutting grains penetrate the workpiece creating grooves that form the surface texture. An approach to determine the number of effective cutting grains and corresponding active area (Aa) was developed based on analysis of wheel wear. Following test completion, an area encompassing both worn and unused (grits in new condition) sections of the grinding points were scanned using the Alicona. The level of the highest worn grain was used to establish a baseline plane that was overlaid on the unworn region of the tool. Grains protruding above this plane were considered active, see Fig. 10a. The areas highlighted with active grits were calculated (see Fig. 10b) and divided by the equivalent area of a grain (A_p reported in Section 3) to determine the number of effective cutting grits. The percentage of the active areas was also established and the results listed in Table 1.

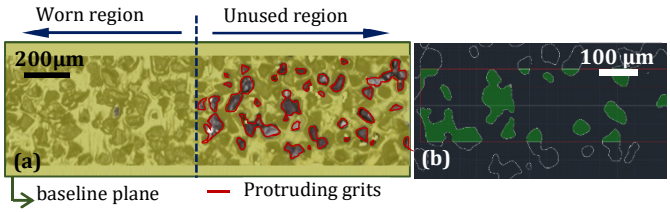

Fig. 10. (a) Tool surface contour showing baseline plane over worn and unused region and protruding grits; (b) Measured area with active grits.

Table 1
Effective cutting grains and active area for each grinding point.

	B76	B46	B32
Active area, Aa (%)	20.2	13.2	18.3
Effective cutting grains (grits/mm²)	48	39	93

Grinding points with higher active areas and in the absence of uneven wear distribution/major tool runout, typically resulted in lower workpiece surface roughness (B76 tool: 20.2% A_a and 0.9 µm Ra; B32 tool: 18.3% A_a and 0.8 µm Ra). Although the number of effective cutting grains in the B32 tool (93 grits/mm²) was significantly higher than the B76 (48 grits/mm²), the difference in ground workpiece surface roughness (Ra) generated by the respective tools was less than ~10%. This is attributed to both the B76 and B32 tools having a similar area of abrasives engaging with the workpiece during operation (comparable active areas).

5. Conclusions

The lowest workpiece surface roughness (Ra) of ~0.8 µm was achieved using the B32 tools, which also had the longest tool life (~2441 G-ratio). The uniformity of wear distribution characterised by the variation in mean height of grains (Spk) measured around the grinding point circumference together with parameters such as number of effective cutting grits and active area, had the strongest influence on resulting workpiece surface roughness. Conversely, the effect of varying cutting parameters (different undeformed chip thickness and tool-workpiece contact length) on roughness was generally negligible.

Acknowledgements

The authors would like to thank Rolls-Royce plc for financial and technical support provided for the research.

References

[1] Klocke F, Soo SL, Karpuschewski B, Webster JA, Novovic D, Elfizy A, Axinte DA, Tönissen S (2015) Abrasive Machining of Advanced Aerospace Alloys and Composites. *CIRP Annals –Manufacturing Technology* 64(2):581-604.

[2] Aspinwall DK, Dewes RC, Burrows JM, Paul MA (2001) Hybrid High Speed Machining (HSM): System Design and Experimental Results for Grinding/HSM and EDM/HSM. *CIRP Annals-Manufacturing Technology* 50(1):145-148.

[3] Aspinwall DK, Soo SL, Curtis DT, Mantle AL (2007) Profiled Superabrasive Grinding Wheels for the Machining of a Nickel Based Superalloy. *CIRP Annals-Manufacturing Technology* 56(1):335-338.

[4] Curtis DT, Soo SL, Aspinwall DK, Mantle AL (2016) Evaluation of Workpiece Surface Integrity Following Point Grinding of Advanced Titanium and Nickel Based Alloys. *Procedia CIRP* 45(1):47-50.

[5] Kadivar M, Azarhoushang B, Shamray S, Krajnik P (2018) The Effect of Dressing Parameters on Micro-Grinding of Titanium Alloy. *Precision Engineering* 51(1):176-185.

[6] Li LL, Sun YW (2012) Experimental Investigation on Surface Integrity in Grinding Titanium Alloys with Small Vitrified CBN Wheel. *Applied Mechanics and Materials* 117-119:1483-1490.

[7] Beranoagirre A, de Lacalle LL (2013) Grinding of Gamma TiAl Intermetallic Alloys. *Procedia Engineering* 63(1):489-498.

[8] Yan QS, Zhang ZQ (2003) CBN Quill Grinding for 2-dimensional Curved Surface. *Key Engineering Materials* 233:509-514.

[9] Uhlmann E, Klein TB, Koprowski S (2014) Tilt Angle Effects in Surface Grinding with Mounted Points. *Production Engineering* 8(4):431-442.